

Rapid and accurate generation of various concentration gradients using polydimethylsiloxane-sealed hydrogel device

Minseok Kim · Mingjie Jia ·
Youngmi Kim · Taesung Kim

Received: 29 April 2013 / Accepted: 10 September 2013 / Published online: 20 September 2013
© Springer-Verlag Berlin Heidelberg 2013

Abstract We report a microfluidic device that can rapidly and accurately generate various concentration gradients in a controllable manner for the chemotaxis study of motile bacterial cells by integrating hydrogel into polydimethylsiloxane (PDMS) microchannels. We performed numerical simulations for both the PDMS-sealed hydrogel hybrid device and a representative conventional hydrogel-based device to theoretically compare their characteristics. In addition, we experimentally demonstrated that the PDMS-sealed hydrogel device not only produces various linear and nonlinear concentration gradients without flow-induced shear stresses on motile bacterial cells but also exhibits remarkable advantages over conventional hydrogel-based devices. For example, the PDMS-sealed hydrogel device can be used for fast and accurate generation of various concentration gradients, prevents dehydration of hydrogel and evaporation of solutions, directs diffusion of chemicals such as chemoattractants, exhibits long-term durability, and is easy to handle. Because the hydrogel used is biocompatible and arbitrary concentration profiles can be easily designed and produced on a chip, we believe that not only the PDMS-sealed hydrogel fabrication method but

also the versatile concentration gradient generation device can be used for various studies on interaction between chemicals and cells including bacterial chemotaxis assays.

Keywords Microfluidics · Hydrogel · Polydimethylsiloxane · Concentration gradient · Chemotaxis

1 Introduction

Bacterial chemotaxis is a model that clarifies how cells and microorganisms sense and respond to concentration gradients in chemical environments (Adler 1966; Ahmed et al. 2010b). Apart from the studies on the chemotaxis of surface-adherent cells such as neutrophils (Jeon et al. 2002; Sahai et al. 2011), it is more challenging to study the chemotaxis of motile bacterial cells because they are highly susceptible to convection flow. As a result, direct application of convection flow-based microfluidic devices to study the chemotaxis of motile bacteria is limited and diffusion-based devices have conventionally been preferred to study bacterial chemotaxis (Kim and Kim 2010; Cheng et al. 2007; Ahmed et al. 2010a). The diffusion of small chemoattractant molecules is controlled by using nanoporous, biocompatible materials such as agarose hydrogel (Cheng et al. 2007; Ahmed et al. 2010a; Kim and Kim 2010; Si et al. 2012), polyethylene, polycarbonate, nitrocellulose membranes (Chueh et al. 2007; Kim et al. 2009; Diao et al. 2006), and self-assembled nanoparticles (Choi et al. 2012). However, using such materials is an obstacle to producing various concentration profiles for different chemoattractants. Although laminar flow-based devices have previously been used to quickly generate and tune concentration gradients (Kim et al. 2011; Jeon et al. 2002;

Electronic supplementary material The online version of this article (doi:10.1007/s10404-013-1265-y) contains supplementary material, which is available to authorized users.

M. Kim · M. Jia · Y. Kim · T. Kim (✉)
School of Mechanical and Advanced Materials Engineering,
Ulsan National Institute of Science and Technology (UNIST),
50 UNIST-gil, Eonyang-eup, Ulsan 689-798, Republic of Korea
e-mail: tskim@unist.ac.kr

T. Kim
School of Nano-Bioscience and Chemical Engineering, Ulsan
National Institute of Science and Technology (UNIST),
50 UNIST-gil, Eonyang-eup, Ulsan 689-798, Republic of Korea

Gorman and Wikswo 2008; Englert et al. 2010), convection flow can significantly bias the chemotactic responses of bacterial cells (Hill et al. 2007). For example, *Escherichia coli* (*E. coli*) swim at the speed of approximately 25 $\mu\text{m/s}$ in a static fluid (Kim and Kim 2010) while convection flow seems to be typically $>100 \mu\text{m/s}$ (Kim et al. 2011; Yeh et al. 2011), which may limit the use of convection flow-based devices that can produce nonlinear complex concentration profiles across microchannels in bacterial chemotaxis studies.

Although conventional hydrogel-based (CHB) microfluidic devices (Cheng et al. 2007; Ahmed et al. 2010a; Haessler et al. 2009) effectively eliminate convection flow, they show some limitations. For example, they produce simple (mostly linear) concentration profiles, they exhibit low durability, and (most importantly) the chemoattractants used in CHB devices diffuse out in all directions in the hydrogel regardless of the design of the microchannels. Further, it is difficult to produce complex patterns on hydrogels such as agarose because hydrogels are amorphous, soft materials that mostly consist of water ($\sim 99\%$). In addition, hydrogels easily become dehydrated and the transport of molecules through hydrogels is not well guided in a desired direction. To overcome these limitations, we sealed a hydrogel with PDMS to develop a diffusion-based microfluidic device that generates linear and nonlinear concentration gradients on a chip for bacterial chemotaxis assays. Typically, nonlinear concentration gradients are important to understand the chemical sensing mechanism of motile cells because they are known to sense both an ambient concentration and a concentration gradient simultaneously (Stock 1999; Herzmark et al. 2007; Ahmed et al. 2010a).

Here, we describe a PDMS-sealed hydrogel (PSH) device that encapsulates a thin agarose hydrogel layer between a source and a sink channel with patterned test microchannels in it. We use numerical simulation to compare the PSH device with a representative CHB device and characterize the concentration gradients across the test microchannels to prove the usefulness of the PSH device. Lastly, we also demonstrate that the PSH device can be used to rapidly produce and accurately control various, robust, and stable concentration gradients, facilitating the chemotaxis assays of motile bacterial cells.

2 Methods and materials

2.1 Chemicals and reagents

Green and red food dyes were used to visualize the microfluidic device and diffusion profiles. Fluorescein isothiocyanate (FITC, No. 3326-32-7) of 50 μM in M9

buffer (No. 248510, BD Biosciences) was used to measure the concentration gradient, 1 mM α -methyl aspartate (No. 2792-66-7) was used as a chemoattractant, and Pluronic[®] F-127 (0.02 %) was done as a surfactant. Agarose power (No. 9012-36-6) was dissolved in M9 buffer (1 %) to generate the hydrogel layer. Tryptone broth (TB, 1 % tryptone and 0.5 % NaCl, No. 211705, BD Biosciences) and Luria broth (LB, L3022, BD Biosciences) media were used for cell cultures. Mineral oil (No. M5904) was used to seal the reservoirs in order to prevent dehydration of the hydrogel and evaporation of the fluid. All the chemicals and reagents were purchased from Sigma-Aldrich Corporation unless otherwise noted.

2.2 Preparation of bacterial cells

We used *E. coli*, a motile bacterium, to measure the chemotactic responses in the presence of concentration gradients. The MG1655 strain was transformed with plasmids that contain a constitutive promoter (pLtetO-1) and green fluorescent protein (GFP) genes to quantitatively analyze the chemotactic responses of *E. coli* and determine whether our device was suitable for studying bacterial chemotaxis or not. A single colony of *E. coli* grown on an LB agar plate was inoculated into 5 mL of the motility buffer (TB), which was subsequently shaken at 180 rpm and incubated at 32 °C for 12 h in a rotary incubator. The cells were then centrifuged at 5,000 rpm for 2 min, the supernatant liquid was poured off, and the pelleted cells were resuspended in M9 media. A final optical density at 600 nm wavelength was gauged to ~ 0.4 . Chemotaxis assays were then performed. More detailed information about how the bacterial cells were prepared is described in our previous work (Kim and Kim 2010; Kim et al. 2011).

2.3 Fabrication and operation of microfluidic device

Standard photolithography was used to fabricate the multi-depth microfluidic device (Qin et al. 2010). SU-8 (Microchem 2025, Newton, MA, USA) was first spin-coated onto a Si wafer as thick as 15 μm , baked, and then exposed to UV light using the first photomask for a shallow microfluidic channel network (MA6, Sussmicrotec, Germany). And then, the same fabrication process such as spin-coating, baking, and exposure was repeated for a deep microfluidic channel network (30 μm) by using the second photomask. Figure S1 in the online supplementary information (OSI) shows a dual-level master. The exposure dose for the first and second photomasks was 150 mJ/cm^2 , respectively. The processed Si wafer was subsequently developed, resulting in a dual-level master, which was silanized using trichloro(3,3,3-trifluoropropyl)silane (Sigma-Aldrich, Republic of Korea). PDMS devices were

then replicated in the same manner as in our previous work (Kim et al. 2013; Kim and Kim 2010). In parallel with the preparation of PDMS devices, PDMS prepolymer was uniformly spin-coated (spin-1200D, MIDAS SYSTEM, Republic of Korea) at 500 rpm onto a glass substrate. The PDMS prepolymer-coated substrate was then cured in a convection oven at 65 °C for over 1 h to produce a 1-mm-thick PDMS slab, which was then directly bonded to the PDMS devices through oxygen plasma treatment (50 sccm O₂, 50 W for 3 s, Cute-MP, FemtoScience, Republic of Korea). This process was performed to confer a homogeneous surface property on all the microchannels and very important to facilitate load the agarose hydrogel into the microchannels.

As shown in Fig. 1a, the microfluidic channel network mainly consisted of three parts: chemical-loading (i.e., source and sink) channels, a cell-loading (i.e., test) channel, and hydrogel-loading channels. The “source” channel is the chemical-loading channel that is flushed with a buffer medium containing a chemoattractant. The “sink” channel is the chemical-loading channel that is flushed only with the buffer medium. Therefore, the source and sink channels are used to maintain the fixed boundary conditions of the chemoattractant, resulting in a linear concentration gradient that is perpendicular to the chemical-loading channels (A–A’). The cell-loading channel was designed as a test channel in which various linear and nonlinear concentration profiles could be generated. The fluid flow was stopped

after the cell-loading channel was filled with bacterial cells and a stationary state was maintained to completely eliminate any effects of convection flow on the generated concentration profiles and the chemotaxis of the bacterial cells.

As shown in Fig. 1b, the deep (30 μm) and shallow (15 μm) microchannels were fabricated using PDMS, that is, the hydrogel-filling (test) channel was designed to be shallow while the other channels (including the test channel) were designed to be deep in order to selectively fill the hydrogel layer with a hydrogel precursor solution. The device was heated on a hot plate at 55 °C and a hydrogel solution that had been maintained in a hot water bath (65 °C) was then loaded through the inlets of the middle chamber to fabricate a hydrogel diffusion layer between the source and sink channels. As shown in Fig. 1c, a fluorescein-containing hydrogel solution was gradually squeezed into the middle channel and completely filled it to construct the hydrogel layers except for the test channel (dark areas) still showing after 25 s. The device was then removed to a work bench at a room temperature for gelation. The hydrogel solution continued flowing along the shallow channels but did not cross the deep channels because of the surface tension of the hydrogel solution on the oxygen plasma-treated PDMS surface despite the complex, patterned microchannels across the hydrogel layers. After gelation, the surfaces of all the microchannels were subsequently treated with a surfactant solution to minimize

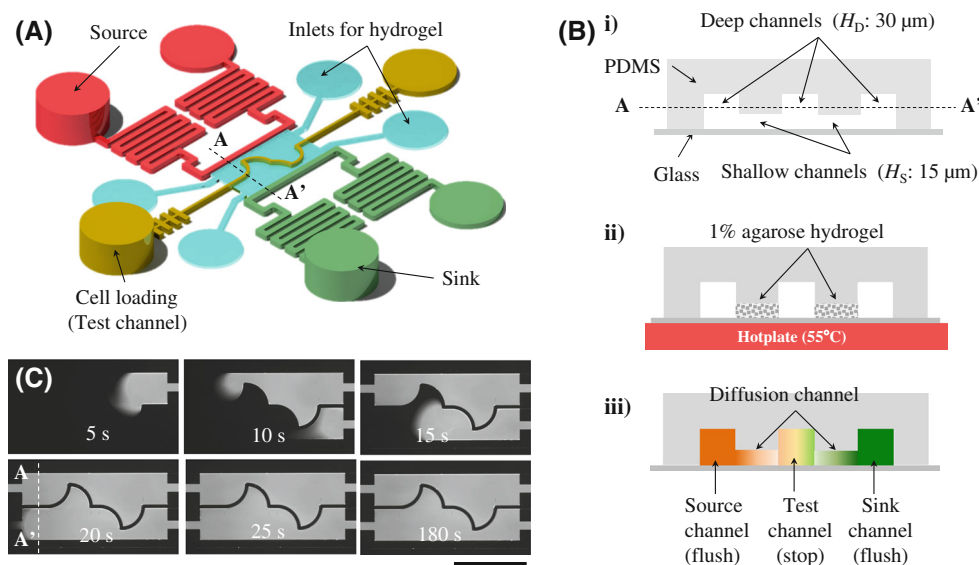


Fig. 1 Concept and fabrication process of the PDMS-sealed concentration gradient generator. **a** Schematic drawing shows that the device consists of an arbitrary test channel in the middle, which is used for cell-loading, two hydrogel-filling channels, and chemical source and sink channels. **b** Generating the concentration gradient in three steps: *i* dual-level, interconnected PDMS microchannels are fabricated; *ii* a hydrogel solution is patterned by using capillary forces to integrate

nanoporous hydrogel into the microchannel; *iii* the source and sink channels are then filled with a chemoattractant and a buffer solution, respectively. **c** Time-lapse fluorescent images show the construction of a hydrogel layer (scale bar 3 mm). This process corresponds to the patterning of hydrogel in **b** and the cross-sectional view of the line A–A’ in **a** and **c** is illustrated in **b**

any nonspecific binding between chemoattractants and the surfaces by flushing the microchannels with 200 μL of the surfactant solution. The residue was rinsed with the M9 buffer solution prior to cell loading.

2.4 Experimental setup and data analysis

An epifluorescence microscope (Ti-U, Nikon, Japan) was equipped with a charge-coupled device (CCD) camera (ORCA R2, Hamamatsu, Japan), 10 \times lenses (focal depth 8.5 μm), and a filter cube (B-2E/C, Nikon) to detect GFP. A confocal microscope (LSM700, Zeiss, Germany) was also used to measure the fluorescence intensities that determined whether a linear concentration gradient was formed along the line A–A' in Fig. 1 that crosses the source channel, the hydrogel layer, the test channel, the hydrogel layer, and the sink channel. Image J (NIH, USA) and Origin 7.1 (OriginLab, Northampton, NC, USA) were used wherever necessary to process images and analyze data, respectively.

2.5 Numerical simulation of diffusion

The transport of small chemoattractant molecules in both hydrogel and buffer solutions can be governed by the transient convection–diffusion equation as follows:

$$\frac{\partial c}{\partial t} + (u \cdot \nabla)c = D\nabla^2 c \quad (1)$$

where c represents the concentration of the chemoattractant, u represents the velocity of the fluid, and D represents the diffusivity of the chemoattractant in the hydrogel or a buffer solution. To study the chemotaxis of the bacterial cells, we forced the convection flow to stop in the test channel so that the flow was negligible across the hydrogels because of the high degree of hydraulic resistance of the nanoporous hydrogel and membrane (Diao et al. 2006). From the experimental conditions and theoretical assumption, u was neglected and an initial condition [$c(x, 0) = 0$] and boundary conditions [i.e., source: $c(x = 0, t) = c_0$ and sink: $c(x = L, t) = 0$] were used for the finite-element method-based simulations using COMSOL Multiphysics (version 4.3a, COMSOL, USA). To quantitatively characterize and compare the PSH device (Fig. 2a) and the CHB device (Fig. 2b), we fixed the source, sink, test channel, ($h_c = 30 \mu\text{m}$ deep, $w_c = 300 \mu\text{m}$ wide) and hydrogel diffusion layer geometries ($h_h = 15 \mu\text{m}$ deep and $w_h = 500 \mu\text{m}$ wide), as depicted in Fig. 2a. The source channel (left) was filled with a chemoattractant solution [α -methyl aspartate 1 mM, $D = 1.4 \times 10^{-9} \text{ m}^2/\text{s}$ in water (Ellegood et al. 2005)] while the sink (right) channel was only filled with water. The same diffusivity, which was assumed to be uniform across the test channel, was used for both models.

The PSH model reached a steady state in 10 min because of the thin, confined PDMS geometry while the CHB model took several hours to reach a steady state as shown in Fig. S2 in OSI. As expected, the chemoattractant molecules diffused much faster in the PSH device than they did in the CHB device. For the PSH model, the concentration of the chemoattractant in the test channel seems to be linear for the entire range of the x -axis and the concentration profile at $t = 10 \text{ min}$ was very close to that when t approached an infinite value. However, for the CHB model, it was almost impossible to produce a linear concentration gradient, although we let the chemoattractant diffuse in this model for a very long time. This can be attributed to the semi-infinite diffusion boundary condition at the source channel. This finding means that the PSH device generates much more accurate linear concentration gradients in the test channel across the hydrogel layer than the CHB device.

Equation (1) is typically simplified as a complementary error function for a transient 1D model as follows:

$$c(x, t) = c_0 \left(\text{erfc} \left(\frac{x}{2\sqrt{Dt}} \right) \right). \quad (2)$$

Therefore, the concentration gradients are theoretically asymptotic with time and the gradients of small molecules gradually become linear when the concentration of the chemoattractant in the sink channel becomes zero as follows:

$$c(x) = c_0 \left(1 - \frac{x}{w_t + 2w_h} \right). \quad (3)$$

Although this approximation has been used for many CHB devices, according to the simulation result, more attention needs to be paid for minimizing errors mainly caused by the diffusion time and boundary effects. In addition to rapidly generating concentration gradients, it is important to consider the linearity of a concentration gradient at the interfaces between the test channel and the hydrogel layer. As shown in Fig. 2c, the PSH model generated a highly accurate linear concentration gradient because the transport of small chemoattractant molecules was well directed and controlled to diffuse across the test channel. In contrast, the CHB model generated a linear concentration gradient only for a narrow region at the center because isotropic diffusion could not be avoided and resulted in the inaccurate formation of concentration gradients (Fig. S2 (D)). The slope of the concentration gradient in the test channel was twice as mild as that of the concentration gradient in the diffusion channel. This is straightforward because the cross-sectional area of the diffusion layer (shallow, middle channel) was fabricated to be twice as shallow as that of the test channel (deep). Because the diffusion mass of the chemoattractant should

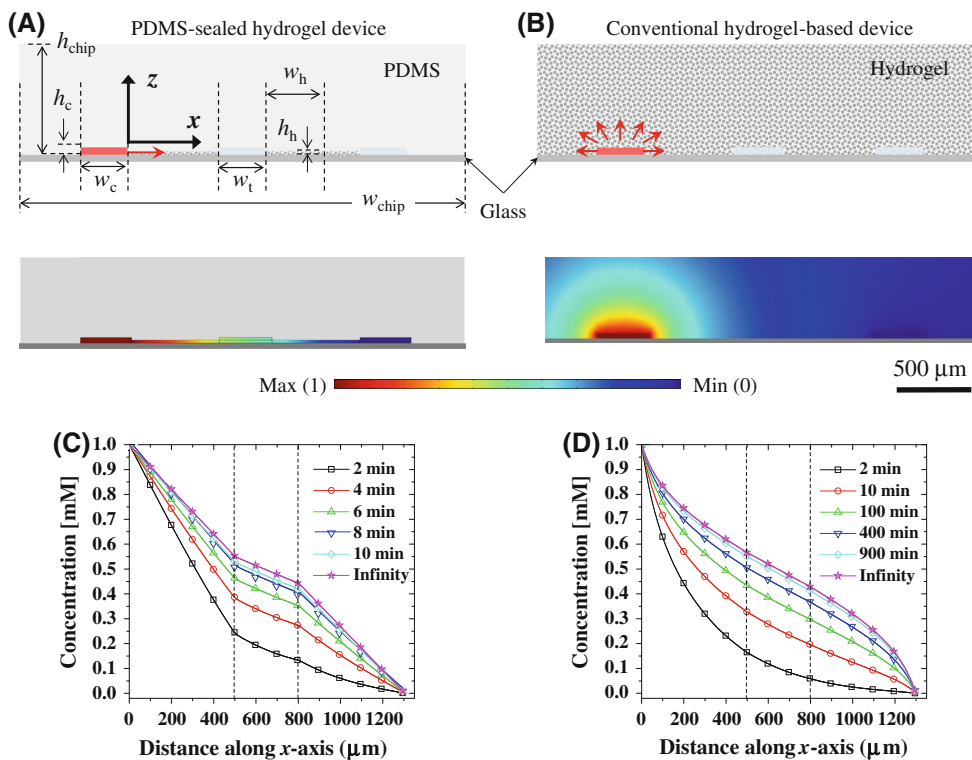


Fig. 2 Numerical simulation of diffusion in a PSH device and in a CHB device. **a** The PSH device shows directed diffusion of small molecules. **b** The CHB device shows isotropic diffusion including molecular transport in undesired directions (illustrations are not to scale). **c, d** The transient concentration distribution profiles computed

from the numerical simulations for **a** and **b**, respectively. The PSH device generates a much more linear concentration gradient and reaches a steady state much more rapidly than the CHB device does. The dimensions of the model are $h_h = 15 \mu\text{m}$, $h_c = 30 \mu\text{m}$, $w_h = 500 \mu\text{m}$, and $w_t = w_c = 300 \mu\text{m}$, and $h_{\text{chip}} = 3 \text{mm}$

be conserved, the concentration of the chemoattractant was halved at the test channel, resulting in a concentration gradient that was twice milder.

It is important to consider whether the concentration gradient in the test channel changes when the test channel is relocated from the center (e.g., from $x = 500 \mu\text{m}$) to the left side (e.g., from $x = 100$ to $400 \mu\text{m}$) of the device. When the test channel was at the center of the device, the slope of the concentration gradient (φ_1) was calculated from Fig. 2c ($1 \text{mM} + \varphi_1 \times 500 \mu\text{m} + \varphi_1/2 \times 300 \mu\text{m} + \varphi_1 \times 500 \mu\text{m} = 0$; therefore, $\varphi_1 = -1/1,150 \text{mM}/\mu\text{m}$); the same result was obtained when the test channel was on the left side and the slope of the concentration gradient was calculated from Fig. S2(D) ($1 \text{mM} + \varphi_2 \times 100 \mu\text{m} + \varphi_2/2 \times 300 \mu\text{m} + \varphi_2 \times 900 \mu\text{m} = 0$; therefore, $\varphi_2 = -1/1,150 \text{mM}/\mu\text{m}$). This is because the diffusion mass along the x -axis should be conserved between the source and sink channel. In fact, this result suggests that the test channel can be relocated anywhere in the hydrogel layer (middle chamber), which enabled us to design an arbitrary test channel to accurately produce nonlinear concentration profiles. Again, the slope of the concentration gradient in the test channel is identical

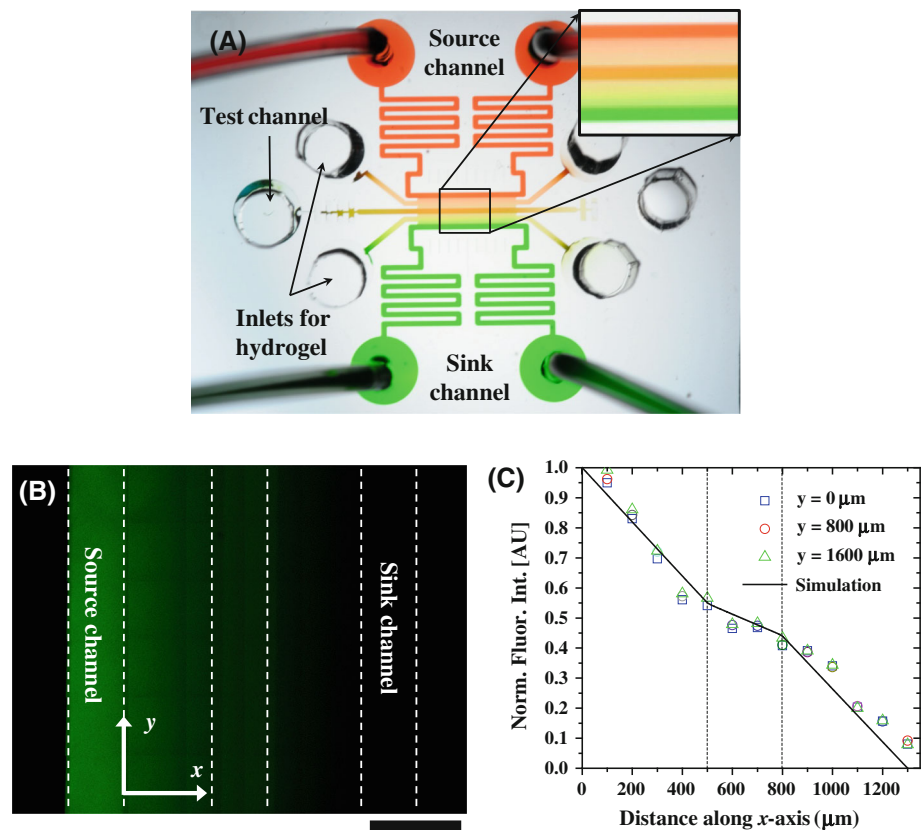
wherever it is located, so nonlinear, arbitrary concentration gradient profiles can be generated as designed. Hence, it is straightforward that diffusion differences along the y -axis in the test channel can be neglected because of the source and sink boundary conditions.

3 Results

3.1 Formation of concentration gradients in PSH devices

We used food dyes and a $50 \mu\text{M}$ FITC solution to test the PSH device. We first injected solutions containing red and green food dyes into the source and sink channels, respectively, and found that fluid does not leak between the hydrogel layer and the PDMS microchannel. As shown in Fig. 3a, the food dyes diffused from the source to the sink channel across the test channel that was filled with only a buffer solution at the center of the device. We performed a similar experiment by replacing the food dye solutions with an FITC solution to quantitatively measure the concentration gradient of the chemoattractant. A regular fluorescence

Fig. 3 Characterization of concentration gradients using fluorescent and food dyes. **a** Colorful image shows that the PSH device generates linear concentration gradients of red and green food dyes, respectively. **b** Confocal microscope image visualizes a linear concentration gradient formed by using a FITC solution. The scale bar is 500 μm . **c** Quantification of the fluorescence intensities of the image in **b** along the x -axis for $y = 0, 800$ and $1,600 \mu\text{m}$, respectively, which is consistent with simulation results (color figure online)



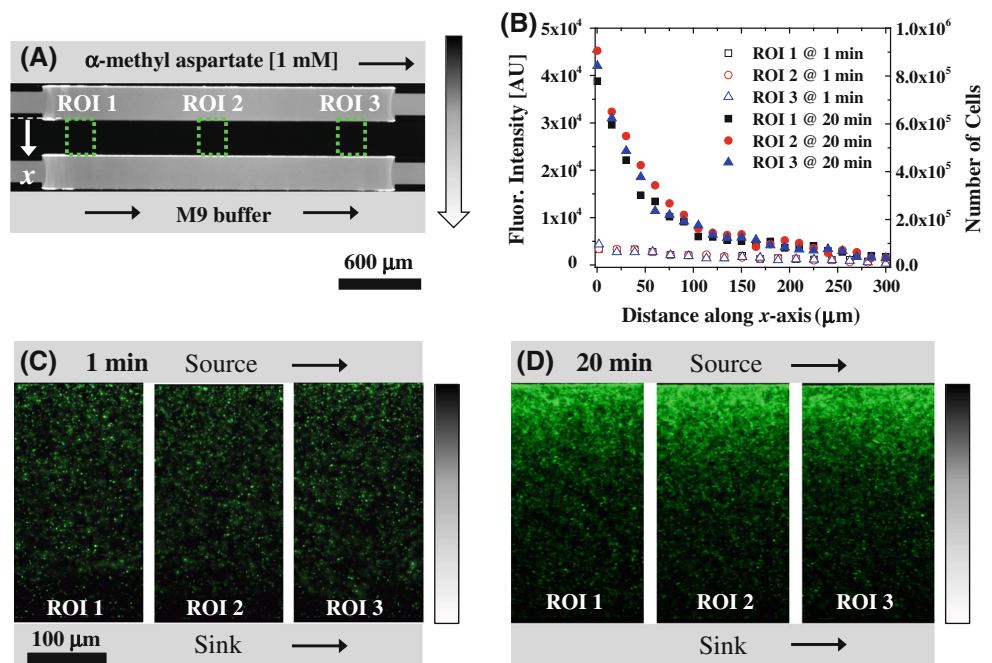
microscope was unsuitable for accurately quantifying the concentration gradient across the hydrogel layer and the test channel because the latter was twice deeper than the former. The fluorescence intensities are typically proportional to the depth of a microchannel when the focal depth is deeper than the microchannel (Fig. S3). To resolve this limitation, we used a confocal microscope to measure the fluorescence intensities. This method provided the real concentration of the chemoattractant across the test channel, as shown in Fig. 3b. The test channel did not show a brighter stripe because the focal depth of the confocal microscope was approximately $2 \mu\text{m}$ while both the hydrogel layer and test channels were much deeper ($>15 \mu\text{m}$) than the focal depth. Figure 3c shows the normalized fluorescence intensities along the x -axis from the source channel across the hydrogel layer to the sink channel. The fluorescence intensities show an almost linear concentration gradient regardless of the position along the y -axis, which is consistent with the theoretical simulation result. Figure S4 (A) shows a fluorescence image taken from the same PSH device used in Fig. 3b by using a fluorescence microscope. The fluorescence intensities quantitatively measured at various positions along the y -axis are also very consistent with each other (Fig. S4 (B)). Furthermore, the concentration gradient was measured daily for a week, demonstrating the long-term durability

and stability of the linear concentration gradient (Fig. S4 (C)). Because the device rapidly generated various stable, durable concentration gradients, we used the concentration gradients to study the chemotaxis of *E. coli*.

3.2 Chemotaxis assays performed using a linear concentration gradient

We used the PSH device to study the chemotaxis of *E. coli*. We fabricated a straight test channel in the middle of the hydrogel layer, as shown in Fig. 4. We loaded an 1 mM α -methyl aspartate solution as a chemoattractant into the source channel and only a buffer solution into the sink channel (Fig. 4a). Subsequently, we waited approximately 20 min for the chemoattractants to diffuse and form a linear concentration gradient and then loaded *E. coli* cells into the test channel (Fig. 4c). Next, we sealed the inlet and outlet reservoirs of the device with mineral oil to balance the hydrostatic pressure, which resulted in the prevention of convection flow in the test channel. Most of the *E. coli* cells migrated toward the high concentration of chemoattractants in the linear concentration gradient. We photographed the fluorescence intensities of the cells and measured the biased chemotactic responses of the cells after 1 min and 20 min, respectively, as shown in Fig. 4c, d. Three regions of interest (ROIs) were arbitrarily determined in the images

Fig. 4 Chemotaxis assay using a linear concentration gradient. **a** Microimage shows experimental conditions generating a linear concentration gradient between the source and the sink channel, two hydrogel layers that contain FITC for visualization, and a straight test channel where cells are loaded and observation was made. **b** Quantification of the fluorescence intensities of the cells migrating toward the high concentrations. **c, d** Fluorescence images taken at 1 and 20 min show the migration of the cells toward the high concentrations



and the fluorescence intensities of the cells in the three ROIs were analyzed. Since the chemotactic responses were distinctly revealed and close to each other, we came to a conclusion that the PSH device is suitable for conducting bacterial chemotaxis assays as shown in Fig. 4b.

3.3 Bacterial chemotaxis assays performed using various nonlinear concentration gradients

We also produced various nonlinear concentration gradients. As shown in Fig. 5a, a linear concentration gradient was produced from the source to the sink channel in the same manner as before. At the same time, various test channels were fabricated in the hydrogel layer. This configuration produced a global, linear concentration gradient while the local concentration gradient depended on the profile of the microchannels. For example, the fluorescence intensities of the FITC solution along line 1, as plotted in Fig. 5b, indicate the formation of a linear concentration gradient. In addition, the concave and convex microchannels produced nonlinear concentration gradients along line 2 and line 3, respectively, and the magnitude of the concentration gradient in line 4 was different from that of the concentration gradients in line 1.

After generating concentration gradients with the chemoattractant in the same manner, we loaded *E. coli* cells into the test channel and then completely stopped the convection flows to observe the chemotactic responses of the cells. Figure 5c shows the various fluorescence intensities of the cells along the concave and convex channels when a global, linear concentration gradient was

maintained throughout the entire period of the assay. For example, the dashed line in yellow in the middle of the image may indicate half the concentration of the chemoattractant in the source channel ($c_0/2$) at a steady state according to Eq. (3). However, the local concentration gradient varies along the channel, that is, the incremental concentrations of the chemoattractant along S_1 continuously increase while they continuously decrease along S_2 (i.e., $|\Delta c/\Delta S_1| > |\Delta c/\Delta S_2|$ for x when $c(x) > c_0/2$). As a result, the cells showed different chemotactic responses, that is, the cells showed stronger positive chemotactic responses in the steep concentration gradient ($|\Delta c/\Delta S_1|$) than in the mild one ($|\Delta c/\Delta S_2|$). The cells in the concave channel (along S_1) show stronger chemotactic responses so that most cells moved to the highest local concentration region in the hydrogel layer. This is why cells are rarely observed in the concave (along S_1) channel compared to the convex channel (along S_2) even though the global concentration of the chemoattractant remains constant. Figure 5d shows the number of the cells along the concave and convex channels. The cells in the concave channel clearly migrated toward the region containing the highest local concentration of the chemoattractant. To confirm this observation, we repeatedly compared the chemotactic responses of the cells to the concentration gradients in the convex and concave channels. Figure 6a shows a wide population band while Fig. 6c shows a narrow, focused one because the steeper concentration gradients in the concave channel attract more cells than the milder ones in the convex channel. Figure 6b, d shows the fluorescence intensities of the cells along the curvilinear channels,

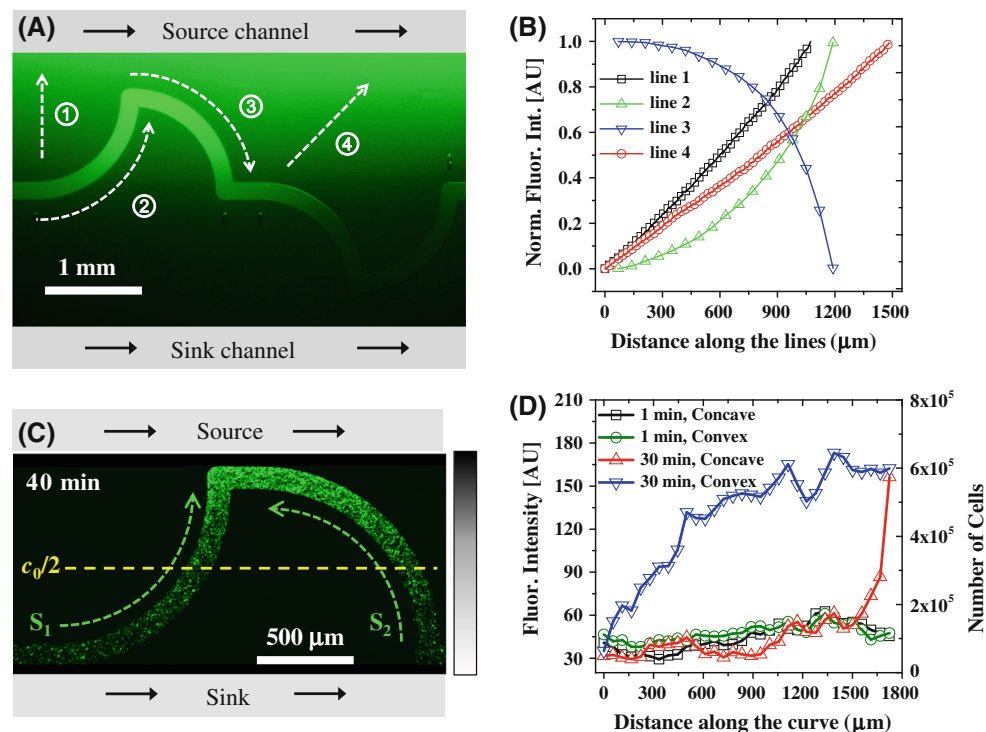


Fig. 5 Characterization of nonlinear concentration gradients and a chemotaxis assay. **a** The microscopic image shows the linear and nonlinear profiles of the concentration gradients of the FITC solution in the test channel. A global, linear concentration gradient is present between the source and the sink channels. **b** Quantification of the fluorescence intensities along the test channels shows various, nonlinear concentration gradients that depend on the shape of the

test channel in the hydrogel layer. **c** The chemotactic responses of the cells in the presence of nonlinear concentration gradients reveal that more cells are attracted to the high-concentration region along S_1 than along S_2 because the local concentration gradient increased more steeply along S_1 than that along S_2 . **d** Quantification of the fluorescence intensities of the cells measured 1 min and 30 min after the assay along S_1 and S_2

demonstrating a potential of highly concentrating a bacterial cell population at a desired location.

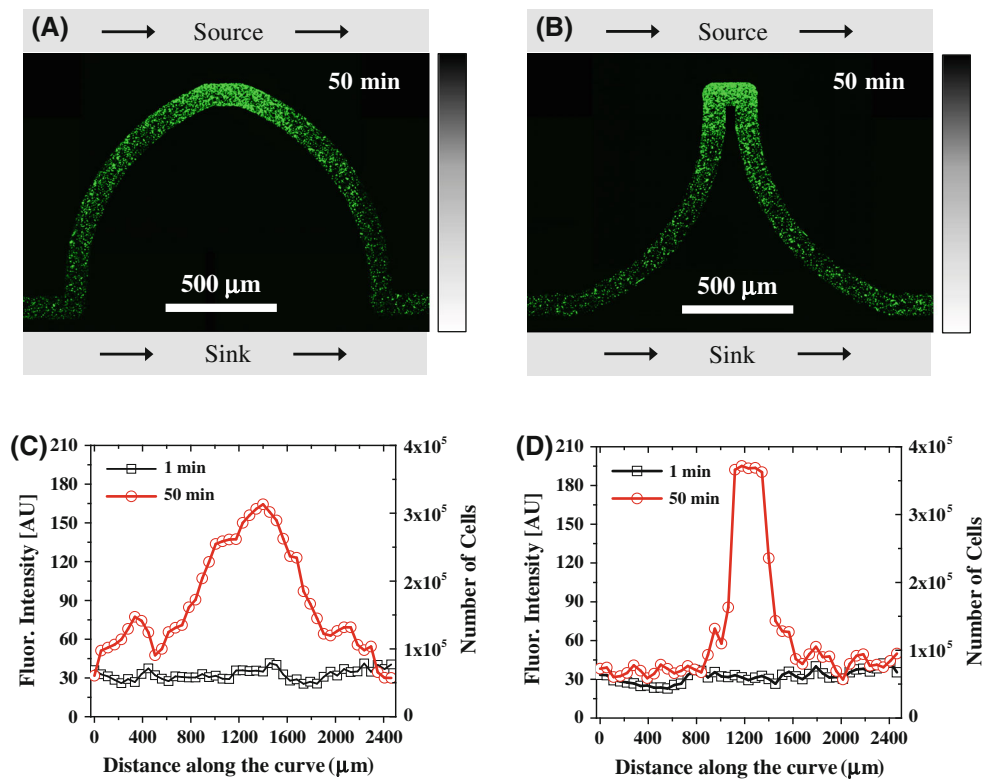
4 Discussion

The PSH device completely resolved the dehydration problem of hydrogels because it encapsulated the hydrogels in the microchannel. From experimental perspective, hydrogels easily dehydrate in CHB devices unless a humidity controller is integrated with them. In addition, the PSH device used a low-density hydrogel (1 %) while CHB devices seem to depend on a high-density hydrogel (3 %). This is because the CHB devices need to handle hydrogel layers without significant deformation. However, the high-density hydrogel decreases the size of the pores in it, dramatically decreasing the effective diffusivity of the hydrogel to less than that of water. For example, the diffusivity of glucose in 1 % agarose is $9.8 \times 10^{-8} \text{ m}^2/\text{s}$, which is very close to the diffusivity of that in pure water, as used in this work. However, the diffusivity of that in 2 % hydrogel significantly decreases to $5.0 \times 10^{-9} \text{ m}^2/\text{s}$ (Lebrun and Junter 1993). We note that the PSH device makes it possible

to much more accurately produce and control concentration gradients, which are more suitable for various bacterial chemotaxis assays. Of course, the low-density hydrogel in the PSH device seems to be susceptible to degradation and infiltration by motile cells. This may alter potentially diffusivity and permeability of chemoattractant molecules over time but we found no defect during the bacterial chemotaxis assays that can be done within several hours.

The motility and density of the cells used for chemotaxis assays in the presence of various nonlinear concentration gradients were at the exactly same condition. This was possible because the hydrogel layer in the PSH device provided enough room to simultaneously produce various concentration gradients by fabricating the concave and convex microchannels. Herein, it would be worth to mention the downside of the test channel. This would be negligible but high motility of bacterial cells may affect the concentration gradient in the test channel by disturbing stationary fluid (swimming). The higher the cell density and motility, the greater errors may be caused. However, the errors can be further minimized once the width of the test channel reduces but is long enough to investigate the chemotactic responses of motile bacterial cells.

Fig. 6 Chemotaxis assays in the convex and concave channels. **a** Convex-like nonlinear concentration gradients caused the cells to migrate toward the highest concentration region, forming a *slightly wide population band*. **b** Concave-like nonlinear concentration gradients caused more cells to be attracted to the highest concentration region, thus forming a *narrow, focused population band*. **c, d** Quantification of the fluorescent intensities along the test channels from *left to right*, respectively



5 Conclusions

The combination of hydrogel and PDMS prevents dehydration of the hydrogel and directs the diffusion/transport of chemoattractant molecules so that various concentration gradients are rapidly produced and accurately controlled without inducing convection flow. Such a device would be more appropriate for conducting chemotaxis assays of motile bacterial cells. In addition, the design concept and advantages of the PSH device over CHB devices were well validated by carrying out numerical simulations. Both the linear and nonlinear concentration gradients were tested by *E. coli* cells that showed a positive chemotaxis toward a chemoattractant by using not only source and sink channels to produce a global, linear concentration gradient between the ends of a hydrogel layer but also a test channel in the hydrogel layer to produce a local, nonlinear concentration gradient. Hence, we believe that the PSH device developed in this work can be widely applied to chemotaxis assays for not only motile microorganisms but also numerous mammalian cells for species screening, drug screening, and/or quantitative biological assays because it more quickly and accurately produces a broader range of concentration gradients that are more versatile, linear, durable, and controllable than those produced using CHB devices.

Acknowledgments This work was supported by a grant from the National Research Foundation (NRF) of Korea (NRF-2009-

C1AAA001-2009-0093479) funded by the Ministry of Education, Science, and Technology by a grant from the Next-Generation Bio-Green 21 program (SSAC, No. PJ00954905), Rural Development Administration, Republic of Korea.

References

- Adler J (1966) Chemotaxis in Bacteria. *Science* 153:708–716
- Ahmed T, Shimizu TS, Stocker R (2010a) Bacterial chemotaxis in linear and nonlinear steady microfluidic gradients. *Nano Lett* 10:3379–3385
- Ahmed T, Shimizu TS, Stocker R (2010b) Microfluidics for bacterial chemotaxis. *Integr Biol* 2:604–629
- Cheng SY, Heilman S, Wasserman M, Archer S, Shuler ML, Wu MM (2007) A hydrogel-based microfluidic device for the studies of directed cell migration. *Lab Chip* 7:763–769
- Choi E, Chang HK, Lim CY, Kim T, Park J (2012) Concentration gradient generation of multiple chemicals using spatially controlled self-assembly of particles in microchannels. *Lab Chip* 12:3968–3975
- Chueh BH, Huh D, Kyrtos CR, Houssin T, Futai N, Takayama S (2007) Leakage-free bonding of porous membranes into layered microfluidic array systems. *Anal Chem* 79:3504–3508
- Diao JP, Young L, Kim S, Fogarty EA, Heilman SM, Zhou P, Shuler ML, Wu MM, Delisa MP (2006) A three-channel microfluidic device for generating static linear gradients and its application to the quantitative analysis of bacterial chemotaxis. *Lab Chip* 6:381–388
- Ellegood J, Hanstock CC, Beaulieu C (2005) Trace apparent diffusion coefficients of metabolites in human brain using diffusion weighted magnetic resonance spectroscopy. *Magn Reson Med* 53:1025–1032

- Englert DL, Manson MD, Jayaraman A (2010) Investigation of bacterial chemotaxis in flow-based microfluidic devices. *Nat Protoc* 5:864–872
- Gorman BR, Wikswo JP (2008) Characterization of transport in microfluidic gradient generators. *Microfluid Nanofluid* 4:273–285
- Haessler U, Kalinin Y, Swartz MA, Wu MW (2009) An agarose-based microfluidic platform with a gradient buffer for 3D chemotaxis studies. *Biomed Microdevices* 11:827–835
- Herzmark P, Campbell K, Wang F, Wong K, El-Samad H, Groisman A, Bourne HR (2007) Bound attractant at the leading versus the trailing edge determines chemotactic prowess. *Proc Natl Acad Sci USA* 104:13349–13354
- Hill J, Kalkanci O, Mcmurry JL, Koser H (2007) Hydrodynamic surface interactions enable *Escherichia coli* to seek efficient routes to swim upstream. *Phys Rev Lett* 98:068101
- Jeon NL, Baskaran H, Dertinger SKW, Whitesides GM, Van de Water L, Toner M (2002) Neutrophil chemotaxis in linear and complex gradients of interleukin-8 formed in a microfabricated device. *Nat Biotechnol* 20:826–830
- Kim M, Kim T (2010) Diffusion-based and long-range concentration gradients of multiple chemicals for bacterial chemotaxis assays. *Anal Chem* 82:9401–9409
- Kim T, Pinelis M, Maharbiz MM (2009) Generating steep, shear-free gradients of small molecules for cell culture. *Biomed Microdevices* 11:65–73
- Kim M, Kim SH, Lee SK, Kim T (2011) Microfluidic device for analyzing preferential chemotaxis and chemoreceptor sensitivity of bacterial cells toward carbon sources. *Analyst* 136:3238–3243
- Kim M, Jia M, Kim T (2013) Ion concentration polarization in a single and open microchannel induced by a surface-patterned perm-selective film. *Analyst* 138:1370–1378
- Lebrun L, Junter GA (1993) Diffusion of sucrose and dextran through agar-gel membranes. *Enzyme Microbial Technol* 15:1057–1062
- Qin D, Xia YN, Whitesides GM (2010) Soft lithography for micro- and nanoscale patterning. *Nat Protoc* 5:491–502
- Sahai R, Cecchini M, Klingauf M, Ferrari A, Martino C, Castrataro P, Lionetti V, Menciassi A, Beltram F (2011) Microfluidic chip for spatially and temporally controlled biochemical gradient generation in standard cell-culture Petri dishes. *Microfluid Nanofluid* 11:763–771
- Si GW, Yang W, Bi SY, Luo CX, Ouyang Q (2012) A parallel diffusion-based microfluidic device for bacterial chemotaxis analysis. *Lab Chip* 12:1389–1394
- Stock AM (1999) A nonlinear stimulus-response relation in bacterial chemotaxis. *Proc Natl Acad Sci USA* 96:10945–10947
- Yeh CH, Chen CH, Lin YC (2011) Use of a gradient-generating microfluidic device to rapidly determine a suitable glucose concentration for cell viability test. *Microfluid Nanofluid* 10:1011–1018